

**Nano-copper Particles-modified Zinc Anode as Protective Coating Enables Dendrite-Free  
Aqueous Zinc Ion Batteries**

Hongchuan Zhu<sup>a</sup>, Mingshu Zhao<sup>a</sup>, Mangmang Shi<sup>a</sup>, Chenjie Yuan<sup>a</sup>, Feng Li<sup>a</sup>, Zhou Su<sup>a</sup>, Lidong Jiao<sup>a</sup>,  
and Min Li<sup>a</sup>

a. School of physics, MOE key Laboratory for Non-Equilibrium Synthesis and Modulation of Condensed  
Matter, Key Laboratory of Shaanxi for Advanced Functional Materials and Mesoscopic Physics, State  
Key Laboratory for Mechanical Behavior of Materials, Xi'an Jiaotong University, Xi'an 710049, China.

---

\*Corresponding authors: E-mail: [zhaomshu@xjtu.edu.cn](mailto:zhaomshu@xjtu.edu.cn);

Tel: +86-13186193932

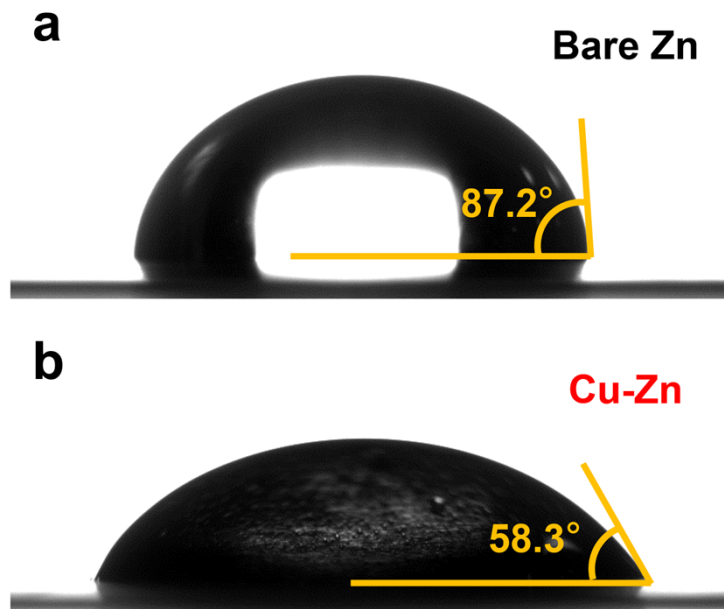


**Fig. S1.** Optical photographs of contact angle tests on (a) Bare Zn and (b) Cu-Zn.

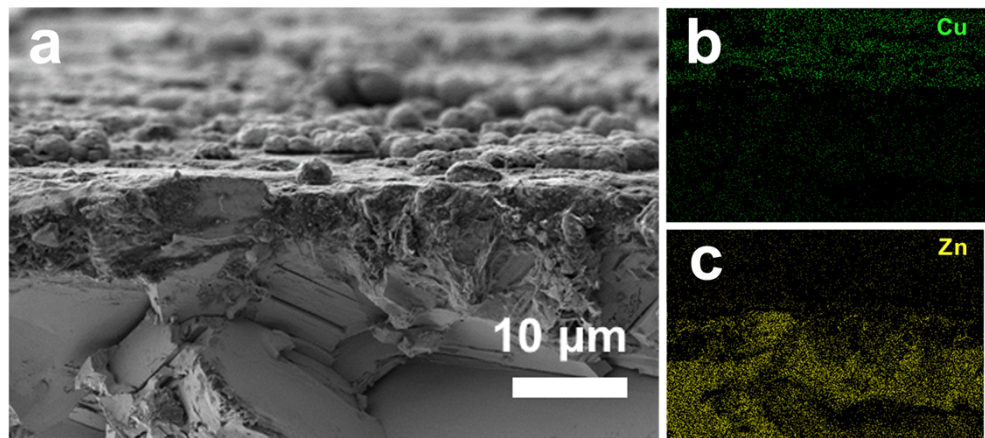


**Fig. S2.** (a) Cross-sectional SEM images of Cu-Zn (brittle fracture after immersion in liquid nitrogen); (b) Cu and (c) Zn elements distribution mapping images of Cu-Zn.

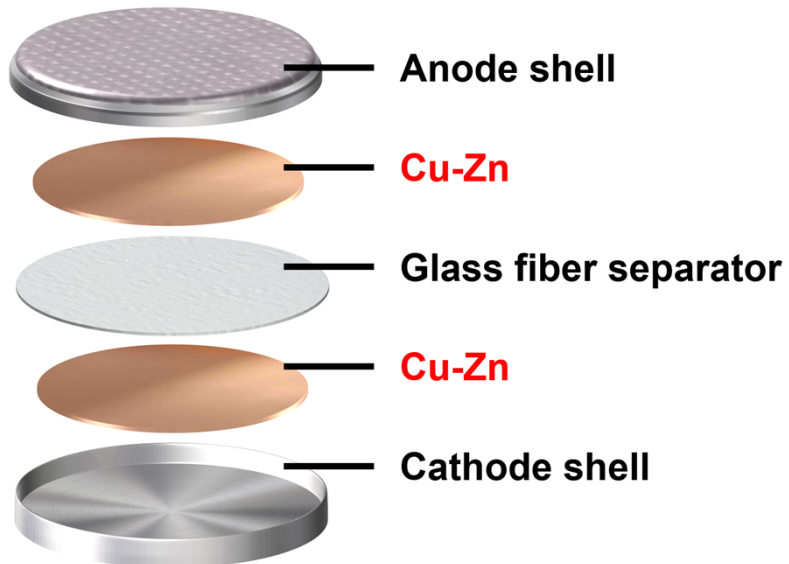


**Fig. S3.** Schematic diagram of the assembly of Cu-Zn||Cu-Zn symmetrical cells.

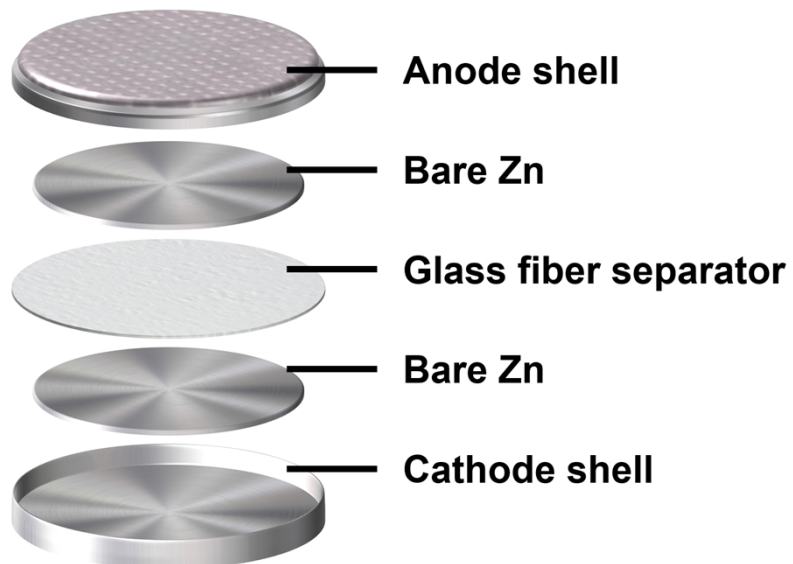


**Fig. S4.** Schematic diagram of the assembly of Bare Zn||Bare Zn symmetrical cells.

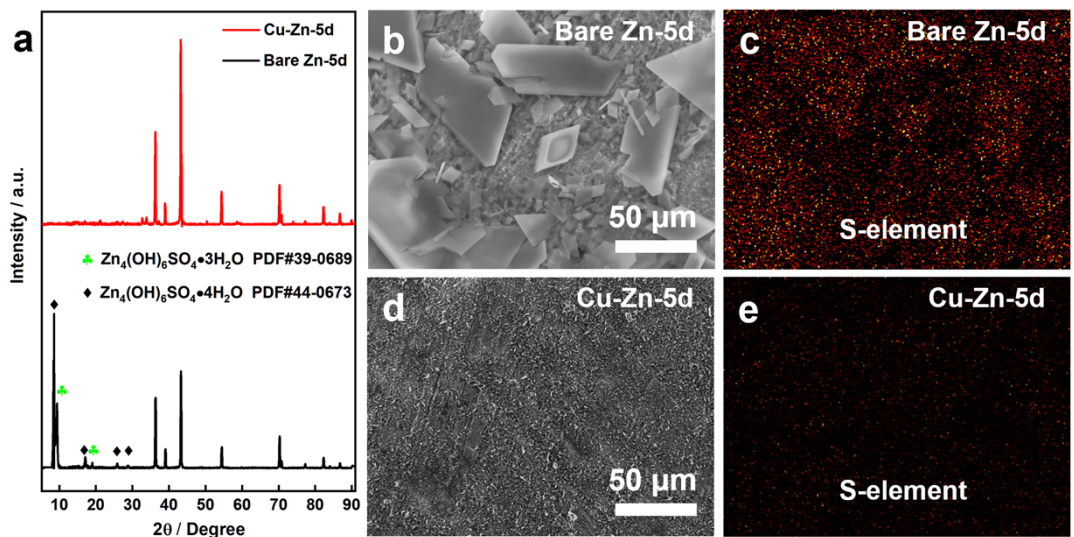


**Fig S5.** Anti-corrosion performance of Bare Zn and Cu-Zn anodes in 2 M  $\text{ZnSO}_4$  electrolyte for 5 days:

(a) XRD patterns of the surface composition of Bare Zn and Cu-Zn anodes after soaking; (b) SEM image and (c) EDS mapping of S element of Bare Zn after soaking; (d) SEM image and (e) EDS mapping of S element of Cu-Zn after soaking.

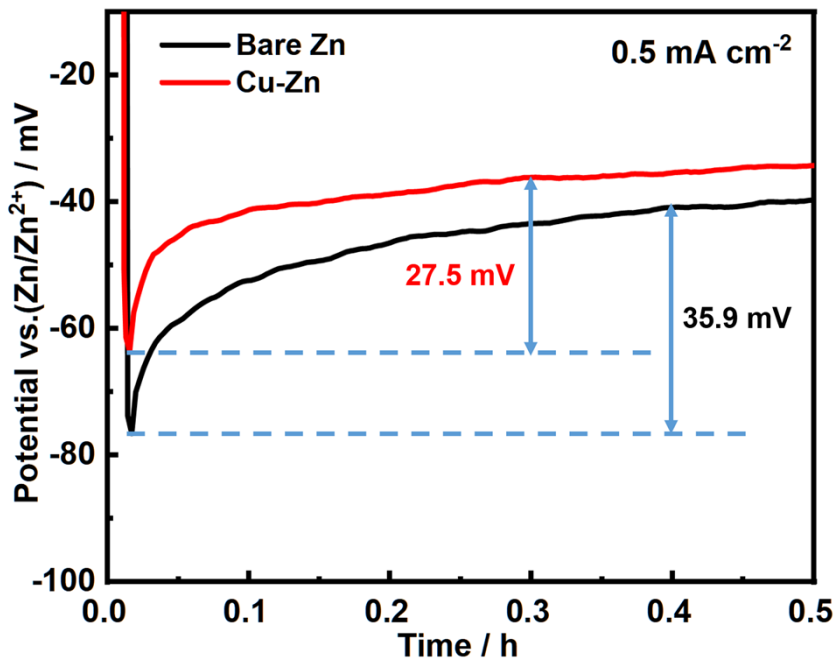


Fig. S6. Overpotential of nucleation at  $0.5 \text{ mA cm}^{-2}$ .

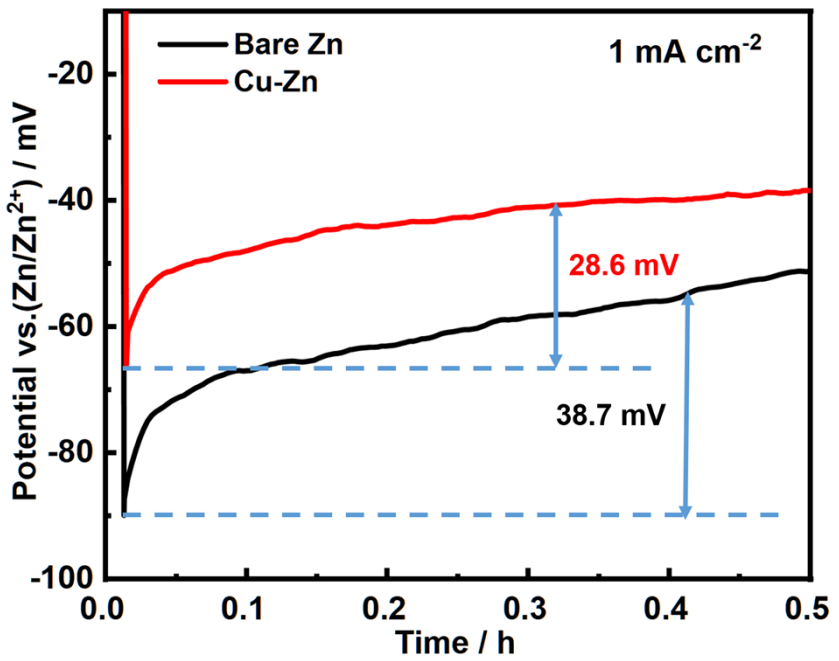
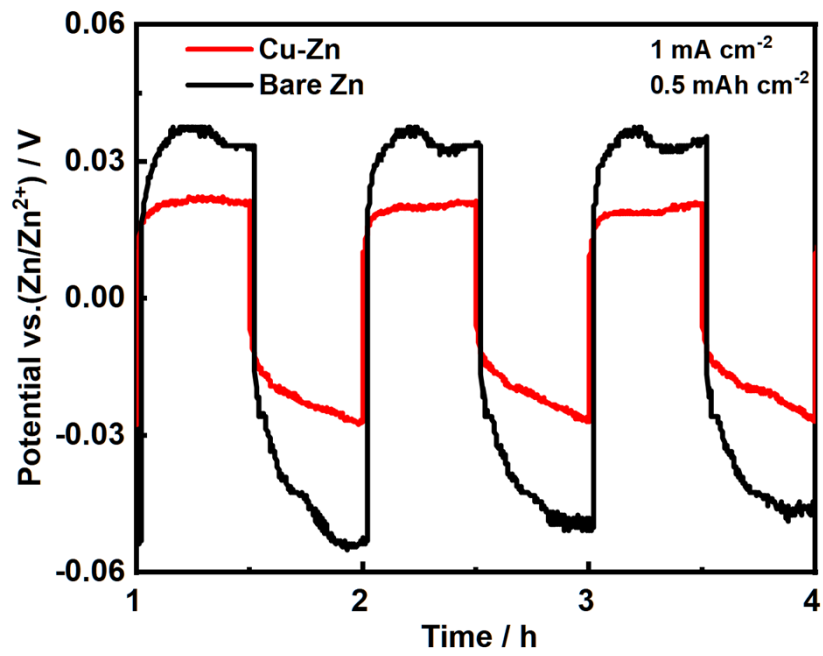
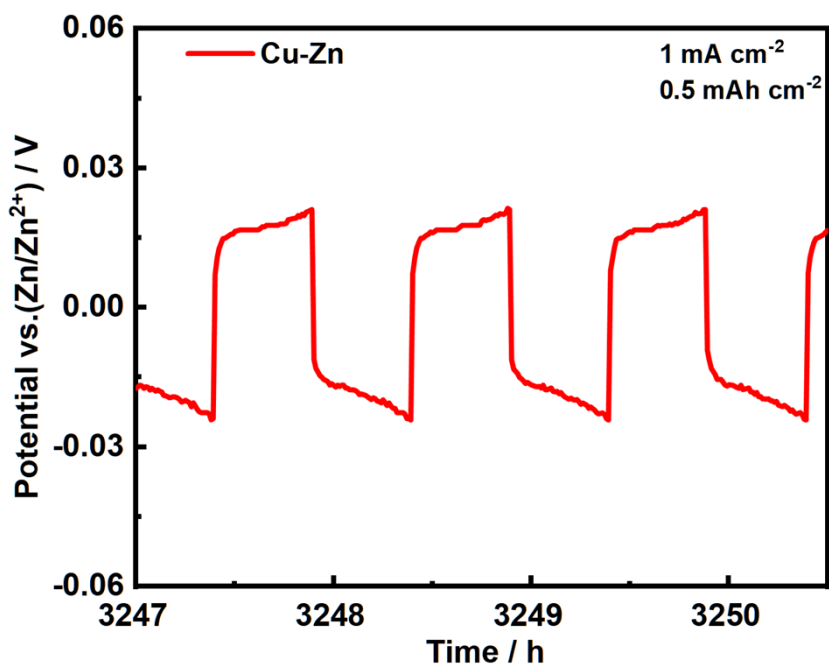


Fig. S7. Overpotential of nucleation at  $1 \text{ mA cm}^{-2}$ .



**Fig. S8.** Initial cycling performance of Bare Zn||Bare Zn and Cu-Zn||Cu-Zn at  $1 \text{ mA cm}^{-2}$  and  $0.5 \text{ mAh cm}^{-2}$ .



**Fig. S9.** Voltage curve of Cu-Zn||Cu-Zn after long-term cycling at  $1 \text{ mA cm}^{-2}$  and  $0.5 \text{ mAh cm}^{-2}$ .

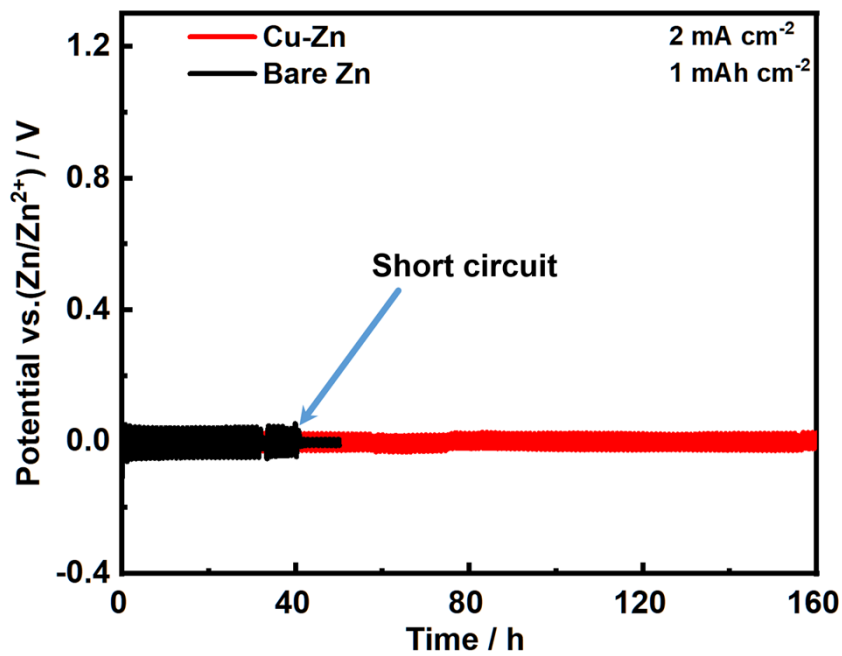


**Fig. S10.** Cycling performance of Bare Zn||Bare Zn and Cu-Zn||Cu-Zn at  $2 \text{ mA cm}^{-2}$  and  $1 \text{ mAh cm}^{-2}$

and (b) its partial amplification diagram at 150-160 h.

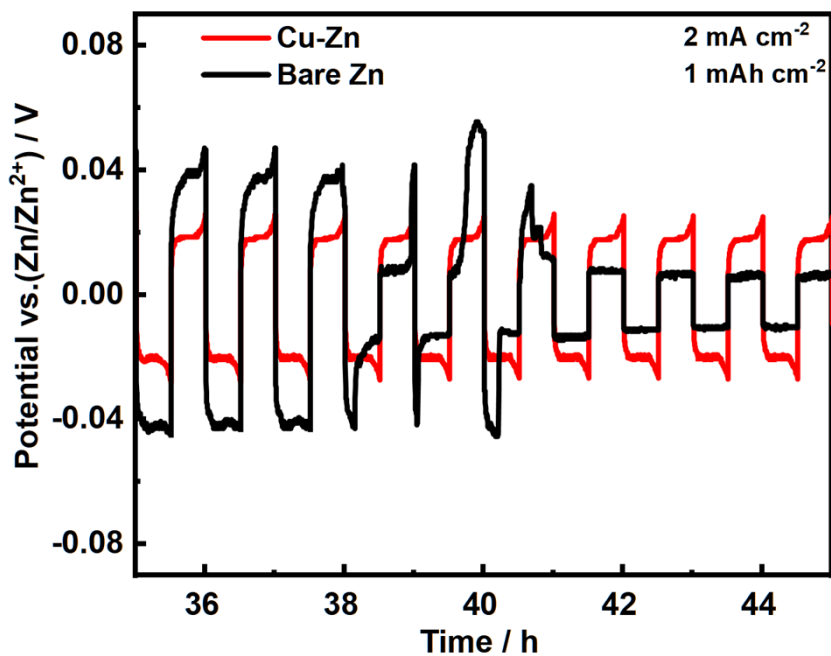


**Fig. S11.** Partial amplification diagram at 35-45 h of Bare Zn||Bare Zn and Cu-Zn||Cu-Zn at  $2 \text{ mA cm}^{-2}$

and  $1 \text{ mAh cm}^{-2}$ .

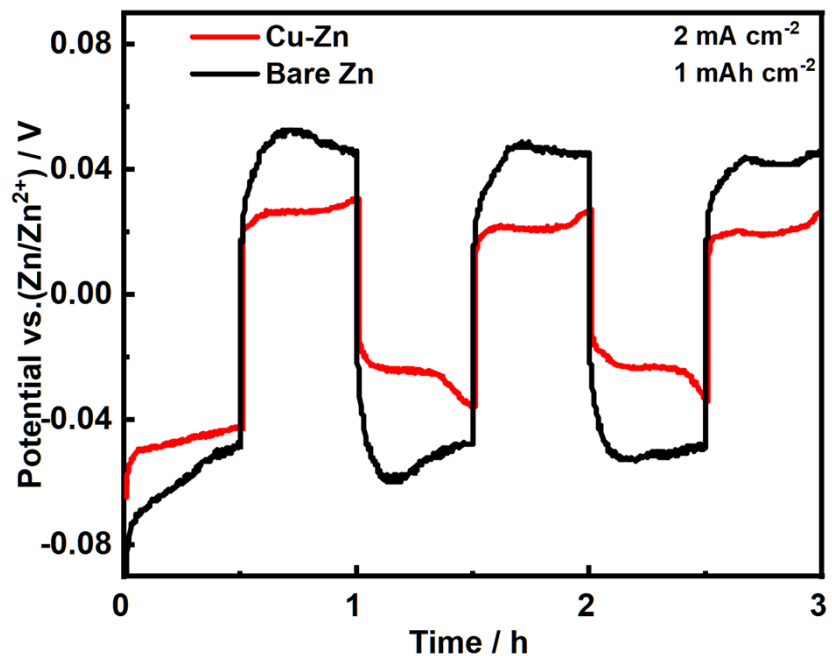


**Fig. S12.** Initial cycling performance of Bare Zn||Bare Zn and Cu-Zn||Cu-Zn at  $2 \text{ mA cm}^{-2}$  and  $1 \text{ mAh cm}^{-2}$ .

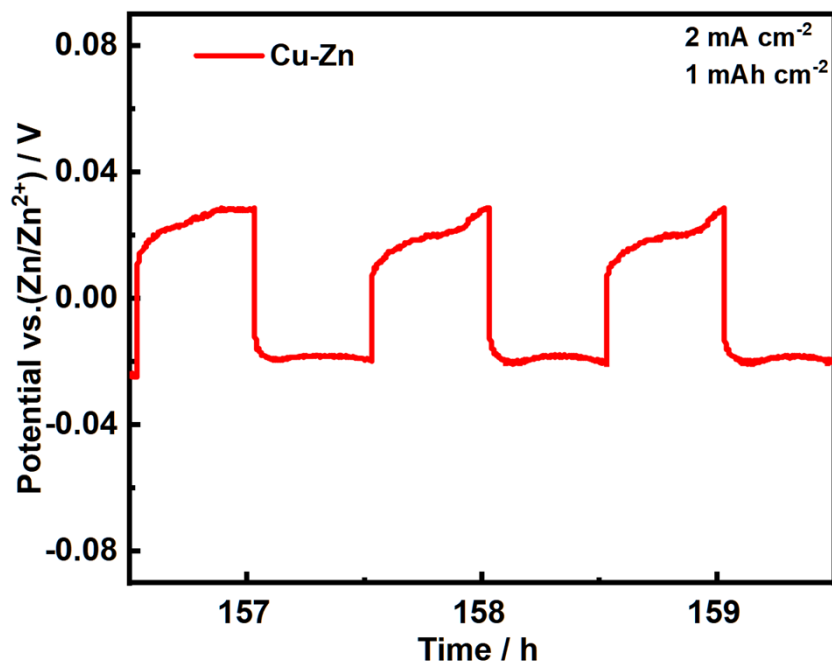


**Fig. S13.** Voltage curve of Cu-Zn||Cu-Zn after long-term cycling at  $2 \text{ mA cm}^{-2}$  and  $1 \text{ mAh cm}^{-2}$ .

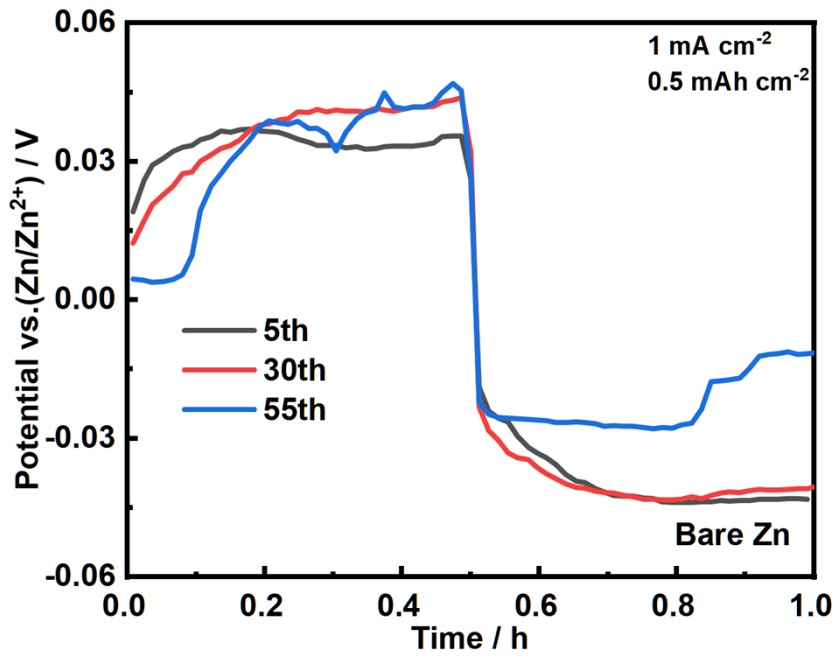


**Fig. S14.** Comparison of voltage curves under different cycles of Bare Zn at  $1 \text{ mA cm}^{-2}$  and  $0.5 \text{ mAh cm}^{-2}$   $\text{cm}^{-2}$ .

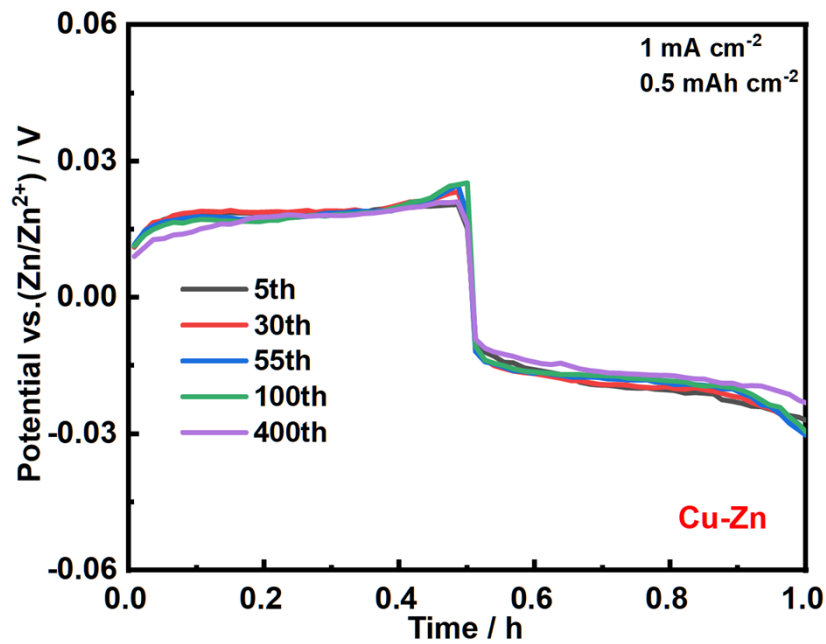


**Fig. S15.** Comparison of voltage curves under different cycles of Cu-Zn at  $1 \text{ mA cm}^{-2}$  and  $0.5 \text{ mAh cm}^{-2}$   $\text{cm}^{-2}$ .

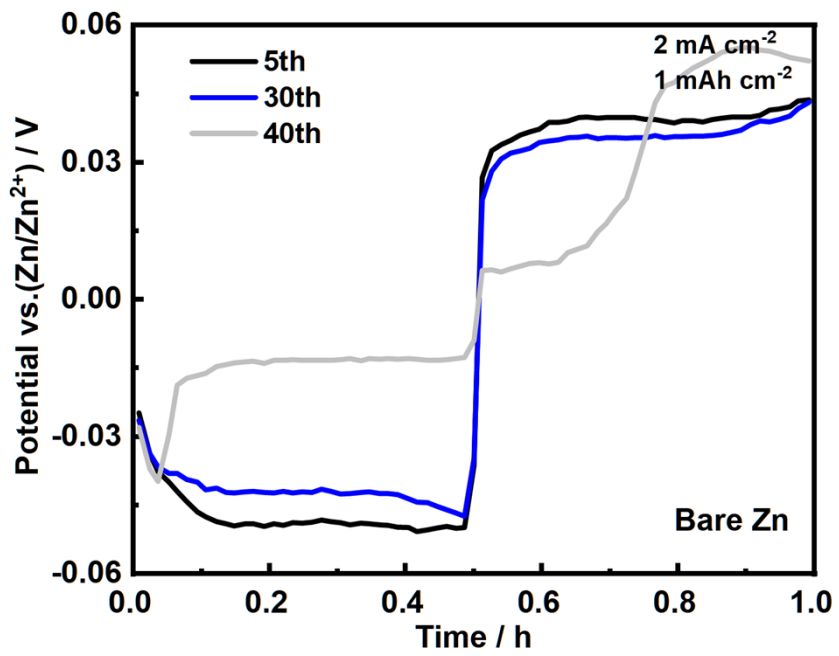


**Fig. S16.** Comparison of voltage curves under different cycles of Bare Zn at  $2 \text{ mA cm}^{-2}$  and  $1 \text{ mAh cm}^{-2}$ .

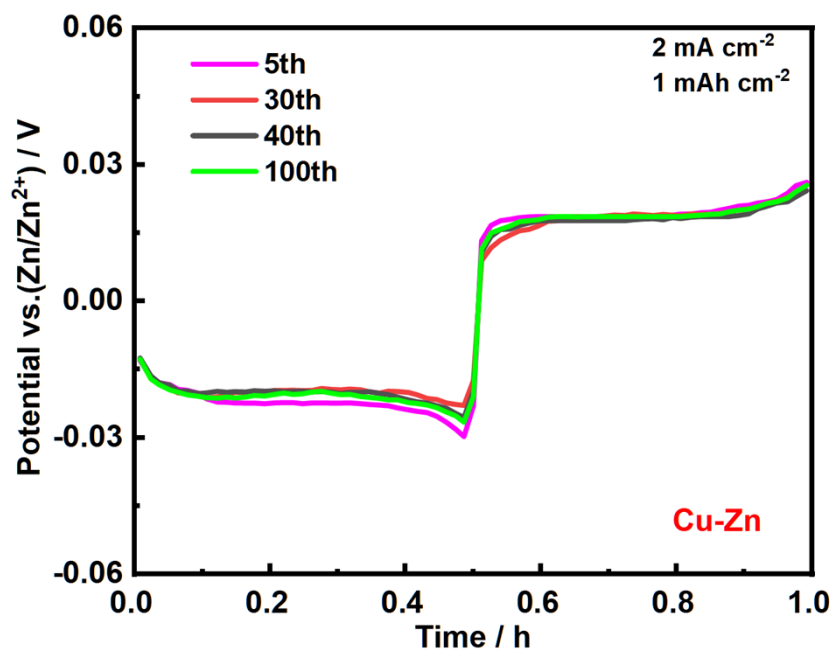


**Fig. S17.** Comparison of voltage curves under different cycles of Cu-Zn at  $2 \text{ mA cm}^{-2}$  and  $1 \text{ mAh cm}^{-2}$ .

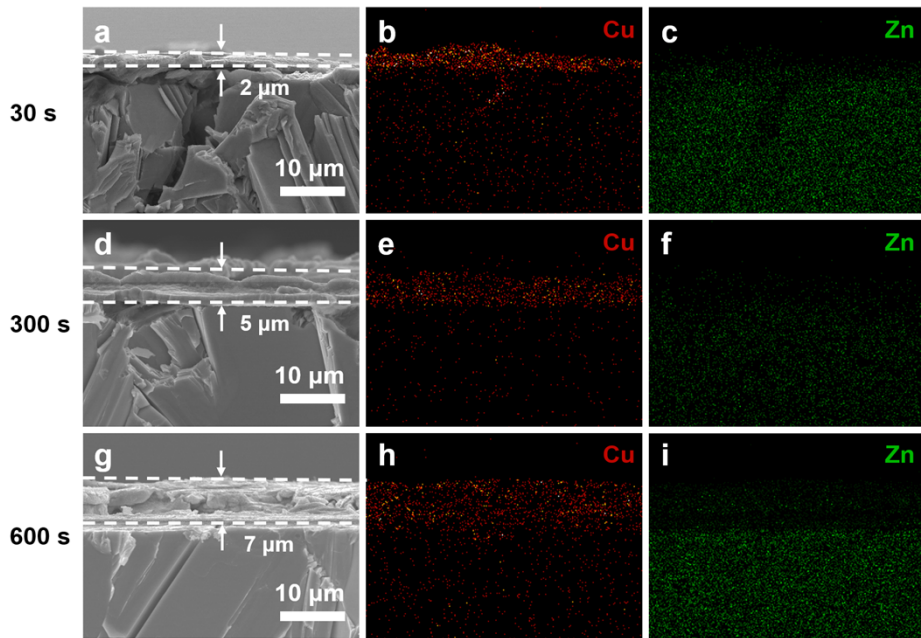


**Fig. S18.** Cross-sectional SEM images and corresponding EDS mapping of Cu-Zn anodes obtained at different reaction times: (a-c) 30 s; (d-f) 300 s; (g-i) 600 s.

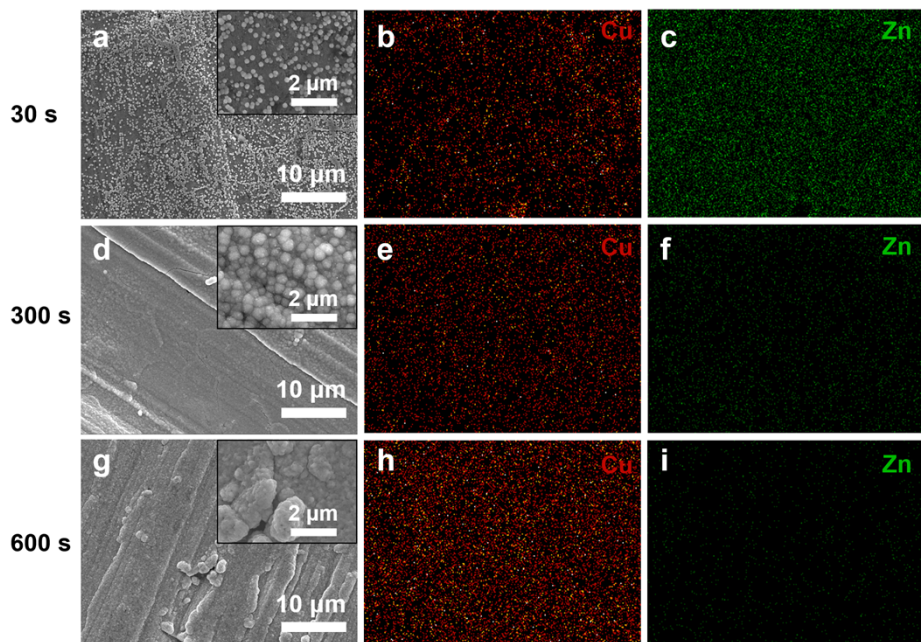


**Fig. S19.** Top-view SEM images and corresponding EDS mapping of Cu-Zn anodes obtained at different reaction times: (a-c) 30 s; (d-f) 300 s; (g-i) 600 s.

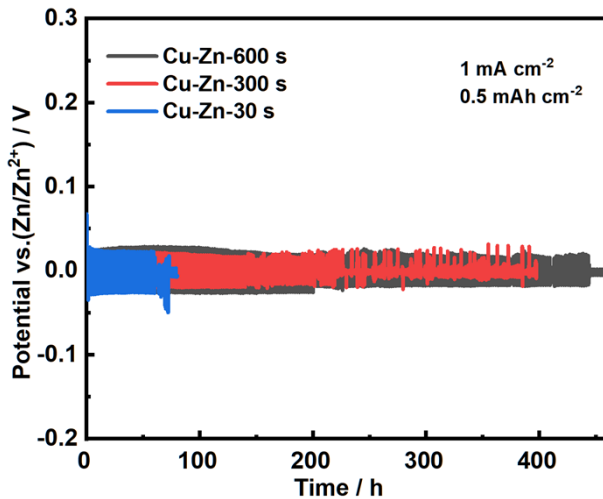


**Fig. S20.** Cycling performance of Cu-Zn anodes obtained at different reaction times at  $1 \text{ mA cm}^{-2}$  and  $0.5 \text{ mAh cm}^{-2}$ : (a-c) 30 s; (d-f) 300 s; (g-i) 600 s. As shown in Fig. S18, when the reaction time is 30s, 300 s, and 600 s, the coverage thickness of the Cu layer obtained is 2 um, 5 um, and 7 um, respectively. The tiny nano copper crystals begin to form initially at a reaction time of 30 s in Fig. S19a-c, sparsely distributed on the surface of Zn. When the time reaches 300 s, copper particles are tightly arranged on the surface of Zn in Fig. S19d-f. Copper particles accumulate irregularly on the surface of Zn when the reaction time is further extended to 600 s in Fig. S19g-i, forming a barrier that blocked further reaction between Zn and the solution. Therefore, it is difficult for the thickness of the Cu layer to increase significantly. Electrochemical tests in Fig. S20 show that symmetrical cells assembled by Cu-Zn-30s, Cu-Zn-300s, and Cu-Zn-600s have cycling life of 70 h, 230 h, and 440 h at  $1 \text{ mA cm}^{-2}$  and  $0.5 \text{ mAh cm}^{-2}$ , respectively. It could be attributed to the weak protection of tiny and sparse cooper particles in Cu-Zn-30s. Moreover, the Cu layer is tightly arranged on the surface of Zn in Cu-Zn-300s and Cu-Zn-600s, which affects the contact between the metallic zinc and the electrolyte, hindering the transport of  $\text{Zn}^{2+}$ . Interestingly, when the reaction time is set to 120 s, the nano-copper particles are homogeneously distributed on the surface of Zn, and a uniform electric field is established by the high conductive copper particles on the surface of Zn, providing unobstructed channels for the transport of  $\text{Zn}^{2+}$ . Therefore, the cycling life of the assembled symmetrical cells can exceed 3200 h under the same conditions, showing extraordinary stability.

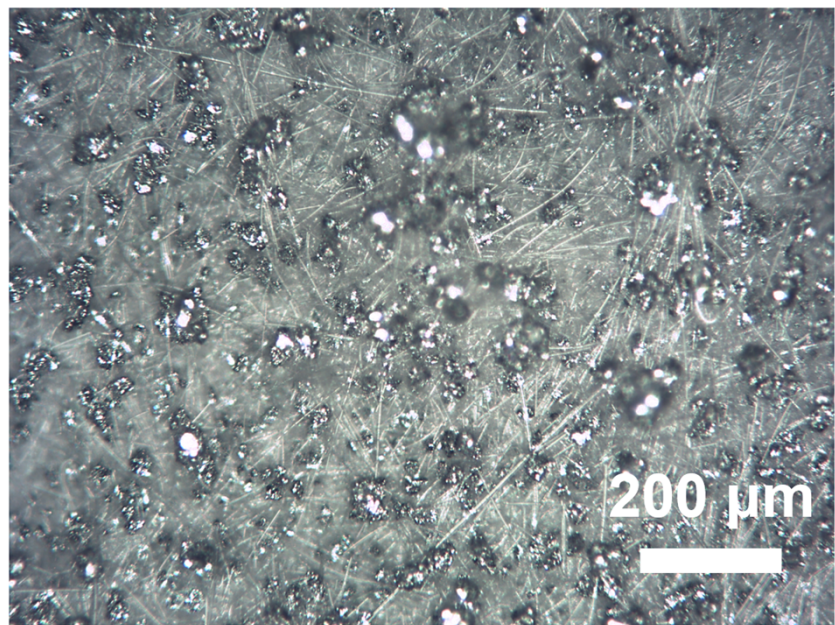


**Fig. S21.** Optical images of Bare Zn after deposition/stripping for 50 h at 2 mA cm<sup>-2</sup> and 1 mAh cm<sup>-2</sup>.

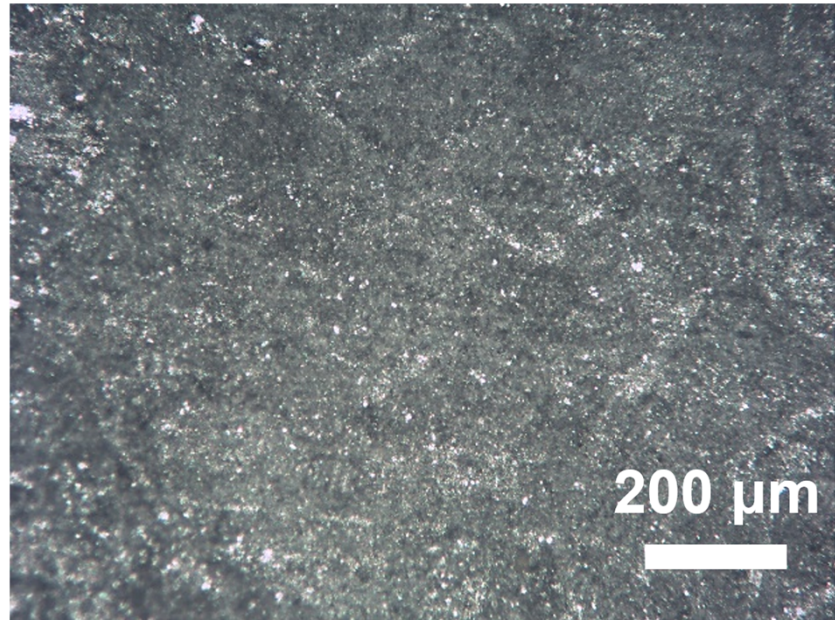


**Fig. S22.** Optical images of Cu-Zn after deposition/stripping for 50 h at 2 mA cm<sup>-2</sup> and 1 mAh cm<sup>-2</sup>.

**Table S1.** Comparison of symmetrical cells based on various modification strategies of zinc anode.

Modification	Current		Average		
	density / mA	Areal capacity / mAh cm <sup>-2</sup>	overpotential / mV	Lifespan / h	Ref.
<b>Cu-Zn</b>	<b>1</b>	<b>0.5</b>	<b>16</b>	<b>3200</b>	<b>This work</b>
Nano Au-Zn	0.25	0.05	83	2000	1
Ag-Zn	1	1	23	350	2
Zn In	1	1	110	510	3
Cu/Zn-Zn	1	0.5	46	1500	4
SiO <sub>2</sub> @Zn	1	0.5	40	1000	5
TiO <sub>2</sub> @Zn	1	1	30	460	6
ZnAl	1	1	42	230	7
PD-Zn	5	1	32	1000	8
Zn-TCPP/Zn	1	1	40	900	9
HNTs@Zn	1	1	39	1005	10
Zn-GZH	1	1	21	1400	11

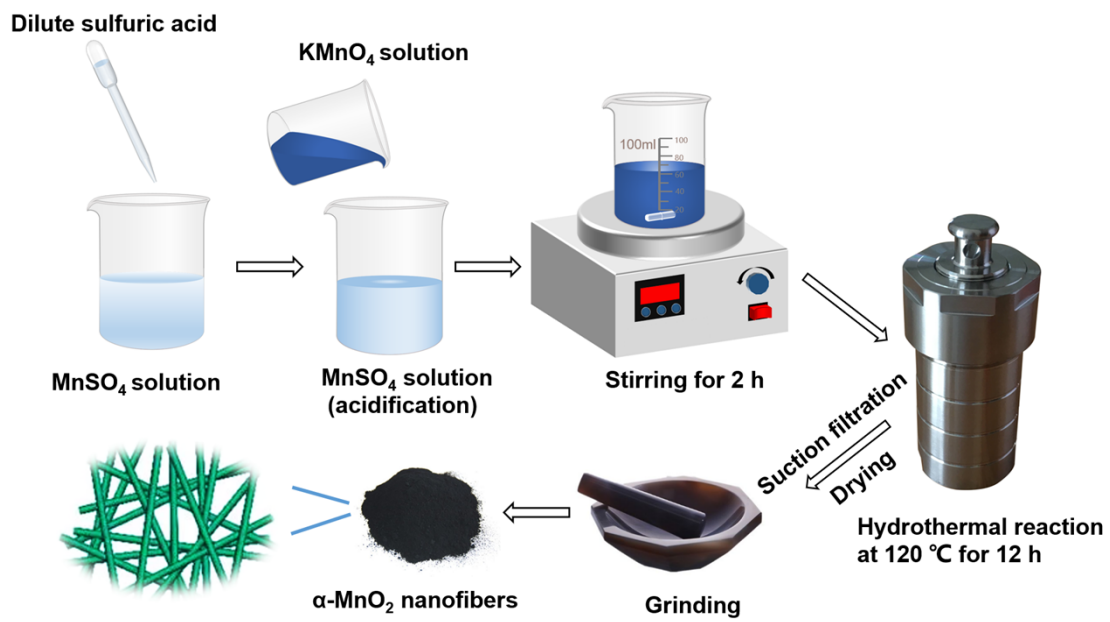


**Fig. S23.** Schematic diagram of  $\alpha$ -MnO<sub>2</sub> preparation.

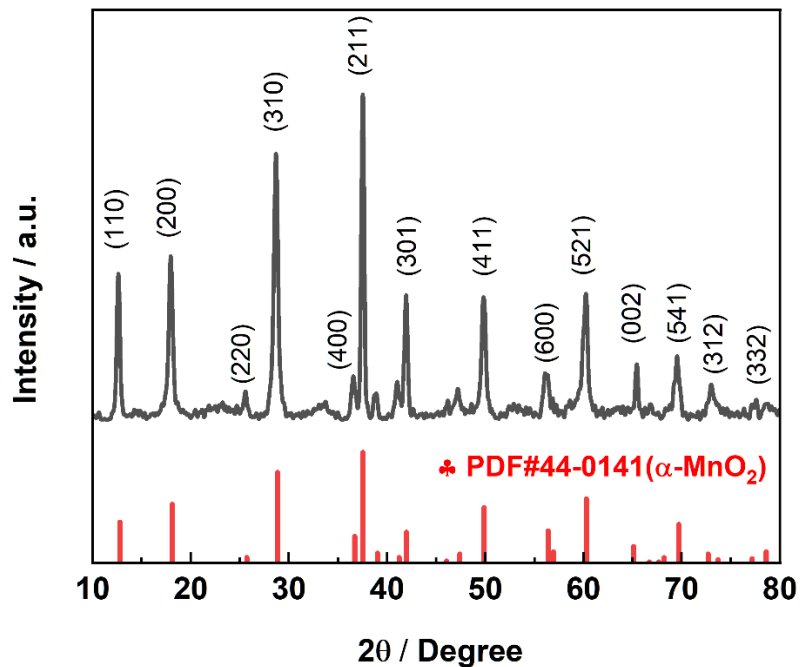


**Fig. S24.** XRD patterns of  $\alpha$ -MnO<sub>2</sub>.

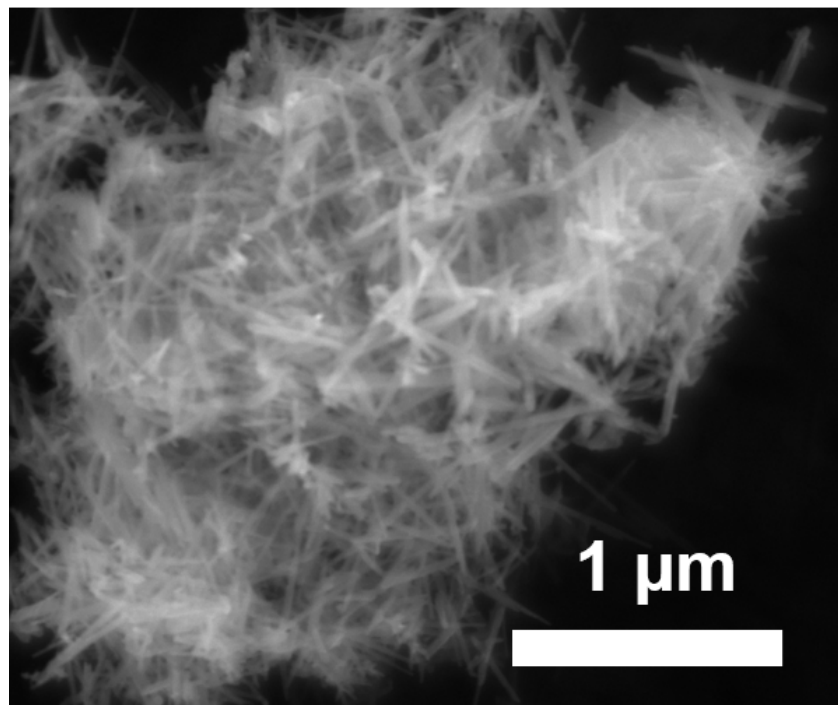


**Fig. S25.** SEM image of  $\alpha$ -MnO<sub>2</sub>.

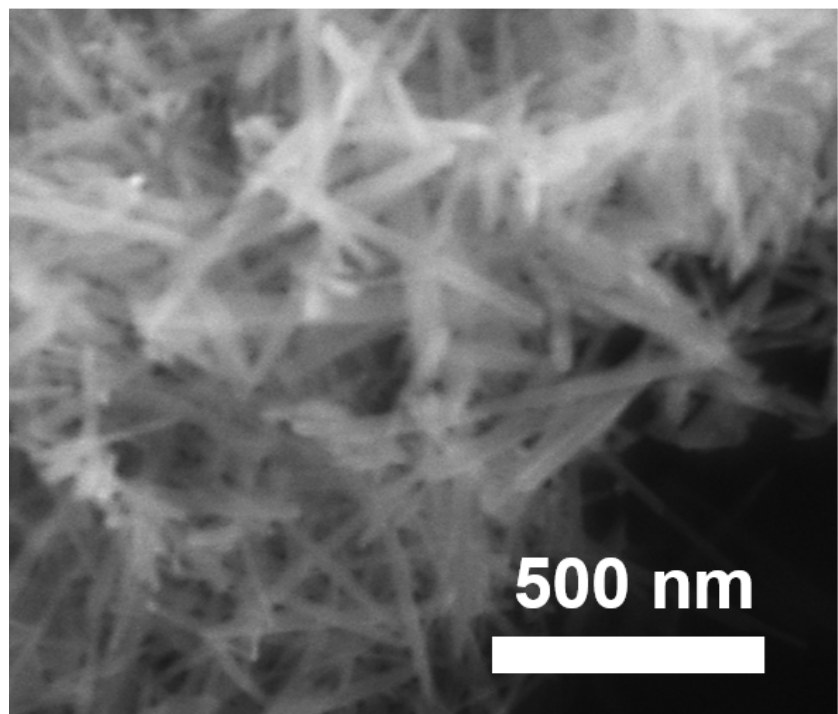


**Fig. S26.** SEM detail magnification of  $\alpha$ -MnO<sub>2</sub>.

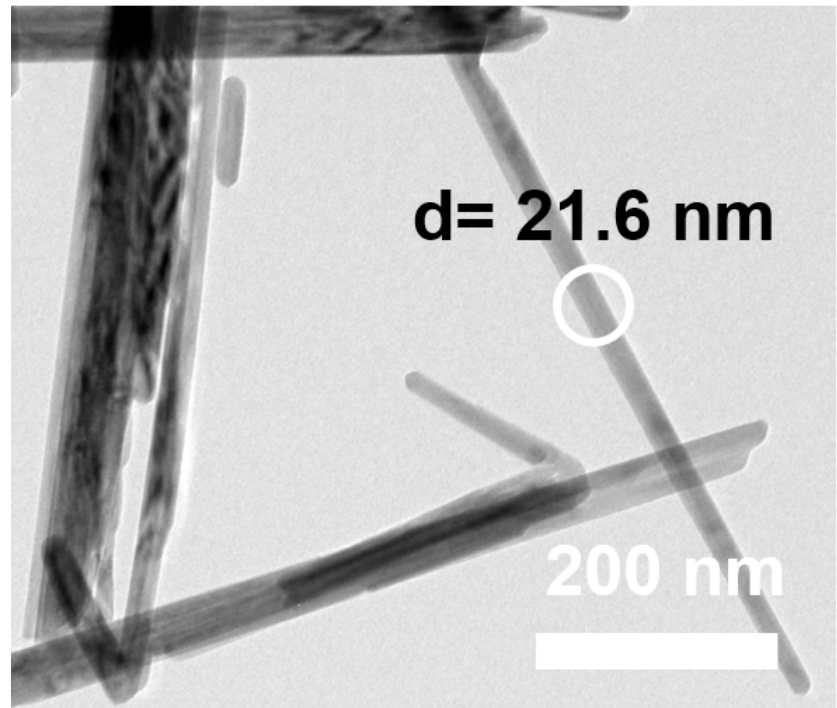


**Fig. S27.** TEM image of  $\alpha$ -MnO<sub>2</sub>.

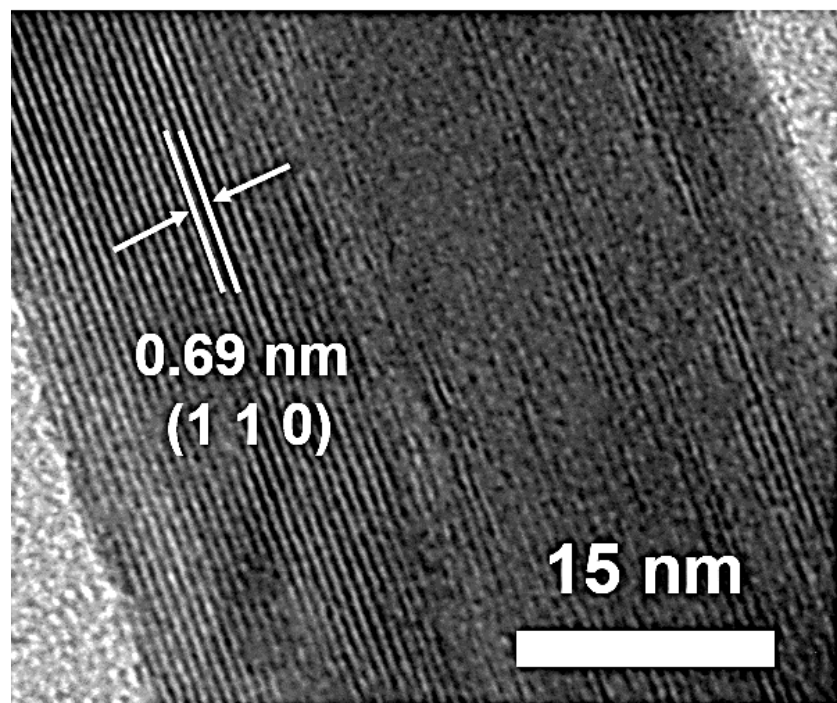


**Fig. S28.** TEM detail magnification of  $\alpha$ -MnO<sub>2</sub>.

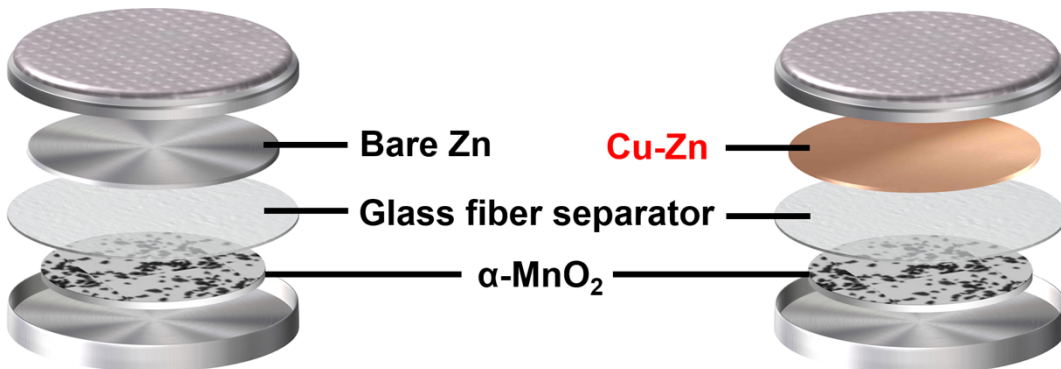


**Fig. S29.** Schematic diagram of the assembly of Cu-Zn|| $\alpha$ -MnO<sub>2</sub> and Bare Zn|| $\alpha$ -MnO<sub>2</sub> full cells.

**Table S2.** Fitting impedance of full cells.

EIS	$R_{ct}/\Omega$	$R_s/\Omega$
Cu-Zn   $\alpha$ -MnO <sub>2</sub>	426.9	1.526
Bare Zn   $\alpha$ -MnO <sub>2</sub>	1498	1.615

## References

- [1] M. W. Cui, Y. Xiao, L. T. Kang, W. Du, Y. F. Gao, X. Q. Sun, Y. L. Zhou, X. M. Li, H. F. Li, F. Y. Jiang and C. Y. Zhi, *ACS Appl. Energ. Mater.*, 2019, **2**, 6490-6496.
- [2] Q. Q. Lu, C. C. Liu, Y. H. Du, X. Y. Wang, L. Ding, A. Omar and D. Mikhailova, *ACS Appl. Mater. Interfaces*, 2021, **13**, 16869-16875.
- [3] D. L. Han, S. C. Wu, S. W. Zhang, Y. Q. Deng, C. J. Cui, L. A. Zhang, Y. Long, H. Li, Y. Tao, Z. Weng, Q. H. Yang and F. Y. Kang, *Small*, 2020, **16**, 2001736.
- [4] Z. Cai, Y. Ou, J. Wang, R. Xiao, L. Fu, Z. Yuan, R. Zhan and Y. Sun, *Energy Storage Mater.*, 2020, **27**, 205-211.
- [5] X. Han, H. T. Leng, Y. Qi, P. Yang, J. X. Qiu, B. Zheng, J. S. Wu, S. Li and F. W. Huo, *Chem. Eng. J.* 2022, **431**, 133931.
- [6] Q. Zhang, J. Y. Luan, X. B. Huang, Q. Wang, D. Sun, Y. G. Tang, X. B. Ji and H. Y. Wang, *Nat. Commun.*, 2020, **11**, 3961.
- [7] Z. C. Qi, T. Xiong, Z. G. Yu, F. B. Meng, B. Chen, H. Xiao and J. M. Xue, *J. Power Sources*, 2023, **558**, 232628.
- [8] Q. Li, A. Chen, D. H. Wang, Y. W. Zhao, X. Q. Wang, X. Jin, B. Xiong and C. Y. Zhi, *Nat. Commun.*, 2022, **13**, 3699.
- [9] F. F. Wang, H. T. Lu, H. Li, J. Li, L. Wang, D. L. Han, J. C. Gao, C. N. Geng, C. J. Cui, Z. C. Zhang, Z. Weng, C. P. Yang, J. Lu, F. Y. Kang and Q. H. Yang, *Energy Storage Mater.*, 2022, **50**, 641-647.
- [10] L. Fan, A. Lin, L. Cao, F. Gu, S. Xiong and Z. Li, *ACS Sustain. Chem. Eng.*, 2022, **10**, 5838-5846.
- [11] J. L. Yang, L. Liu, Z. Yu, P. Chen, J. Li, P. A. Dananjaya, E. K. Koh, W. S. Lew, K. Liu, P. Yang and H. J. Fan, *Acs Energy Lett.*, 2023, **8**, 2042–2050.